Article

Current Biology

# Competition between chemoattractants causes unexpected complexity and can explain negative chemotaxis

## Highlights

- Negative chemotaxis can be mediated by different ligands competing for one receptor
- Mathematical models accurately predict unexpected, counterintuitive cell behaviors
- Ligand competition and breakdown can combine to drive complex outcomes
- Strong and weak attractants can combine to generate repulsive stimuli

## Authors

Adam Dowdell, Peggy I. Paschke, Peter A. Thomason, Luke Tweedy, Robert H. Insall

## Correspondence

robert@chemotaxis.org

## In brief

Competition between different ligands for the same receptor type can explain how cells can drive negative chemotaxis in which cells migrate away from a chemical repellent. Dowdell et al. show that ligand competition and breakdown can combine to cause counterintuitive behaviors, such as two attractants combining to repel cells.

Dowdell et al., 2023, Current Biology *33*, 1704–1715
May 8, 2023 
https://doi.org/10.1016/j.cub.2023.03.006

CellPress

CellPress
OPEN ACCESS

Current Biology

Article

# Competition between chemoattractants causes unexpected complexity and can explain negative chemotaxis

Adam Dowdell,[1,2] Peggy I. Paschke,[2] Peter A. Thomason,[2] Luke Tweedy,[1,2] and Robert H. Insall[1,2,3,4,*]
[1]School of Cancer Sciences, University of Glasgow, Garscube Estate, Glasgow G61 1QH, UK
[2]CRUK Beatson Institute, Switchback Road, Glasgow G63 9AE, UK
[3]Twitter: @robinsall
[4]Lead contact
*Correspondence: robert@chemotaxis.org
https://doi.org/10.1016/j.cub.2023.03.006

## SUMMARY

Negative chemotaxis, where eukaryotic cells migrate away from repellents, is important throughout biology, for example, in nervous system patterning and resolution of inflammation. However, the mechanisms by which molecules repel migrating cells are unknown. Here, we use predictive modeling and experiments with Dictyostelium cells to show that competition between different ligands that bind to the same receptor leads to effective chemorepulsion. 8-CPT-cAMP, widely described as a simple chemorepellent, is inactive on its own and only repels cells when it acts in combination with the attractant cAMP. If cells degrade either competing ligand, the pattern of migration becomes more complex; cells may be repelled in one part of a gradient but attracted elsewhere, leading to populations moving in different directions in the same assay or converging in an arbitrary place. More counterintuitively still, two chemicals that normally attract cells can become repellent when combined. Computational models of chemotaxis are now accurate enough to predict phenomena that have not been anticipated by experiments. We have used them to identify new mechanisms that drive reverse chemotaxis, which we have confirmed through experiments with real cells. These findings are important whenever multiple ligands compete for the same receptors.

## INTRODUCTION

Negative chemotaxis (also called chemorepulsion[1]) occurs when cells are exposed to a spatial gradient of a signaling molecule and move down-gradient, toward the region with the lowest concentration. It is thus the opposite of normal (“positive”) chemotaxis in which cells move up-gradient toward the highest concentration.

Negative chemotaxis is implicated in a wide range of whole-organism processes, including development,[2] immunity,[3,4] disease,[5] and cancer metastasis.[6] For example, neurites in the developing brain avoid areas high in semaphorins,[7] and semaphorin knockout mice die at or before birth.[8] Negative chemotaxis is also considered important for normal immune cell behavior. Neutrophils are attracted to infections and sites of tissue damage by chemoattraction, but when the damage has been resolved they can migrate in reverse, back into the bloodstream.[9] This may be mediated by negative chemotaxis through G-protein-coupled receptors (GPCRs) in particular chemokine and complement fragment receptors, though the environment is complex and distances small, so the precise drivers are not fully understood. The mechanisms behind GPCR-mediated repulsion remain unexplained.

In bacteria, negative chemotaxis is widespread.[10] It works because receptors are tuned by protein methylation to register a “background” concentration of attractant or repellent.[11] If the attractant concentration is higher than the background, the receptor mediates an attractive response; if lower, the response is negative. Thus, one receptor can communicate both positive and negative chemotactic stimuli.

By comparison, eukaryotic chemorepulsion is difficult to explain.[12] Eukaryotic chemotaxis integrates temporal information with spatial data,[13] where the cell compares receptors at different places in the cell. The resulting spatial information is used to steer the cell.[14] Much research has addressed the mechanisms by which attractive receptor stimuli reinforce actin protrusions. The GPCRs that are used in chemotaxis have a wide range of ligand specificities. These varied inputs are integrated at the level of G-protein coupling. When G-proteins are activated, their βγ-subunits positively reinforce local actin polymerization,[15,16] connecting signals from outside the cell to the intracellular processes that control cell movement.

It is difficult to envisage how negative stimuli can be integrated into this type of chemotaxis pathway. G protein βγ-subunits are not thought to be specific, and there is little to suggest that positive and negative stimuli act through different βγ-subunits. Furthermore, when negative chemotaxis has been analyzed in detail, the same receptors promote both positive and negative effects.[1,17] This makes it hard to understand how G-proteins could mediate negative steering. Many eukaryotic

 

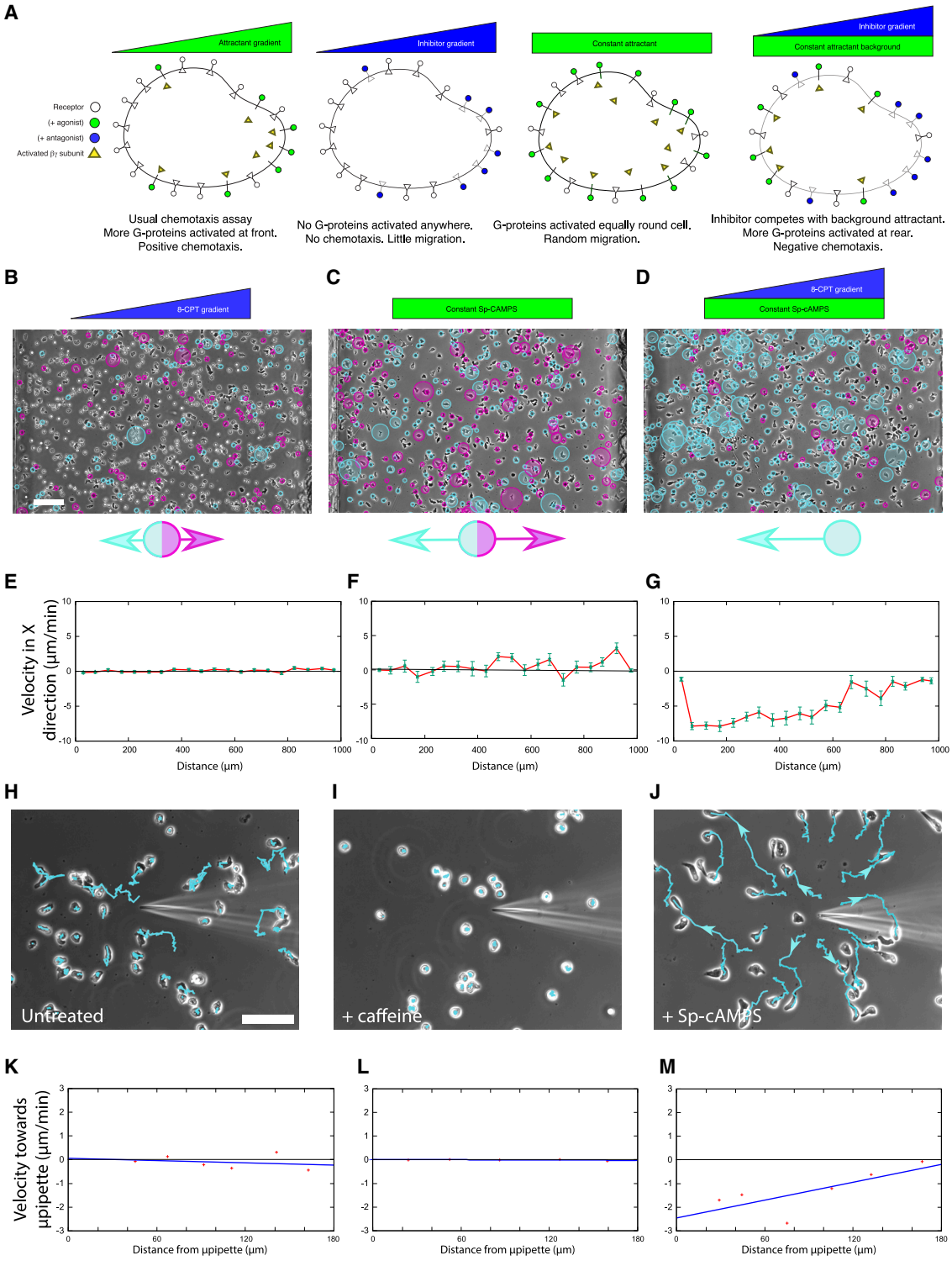


**Figure 1. Repulsion by 8-CPT-cAMP depends on the presence of a competing agonist**

(A) Guidance by receptor competition. Agonists are attractive because a concentration gradient creates a gradient of activated receptors and G-proteins (far left). A similar gradient of antagonists occupies receptors similarly, but does not activate receptors or G-proteins (left). Homogeneous attractant (right) activates receptors and G-proteins, but there is no directional bias so the cells are not steered. A combination of homogeneous agonist and a gradient of antagonists causes a steering in the opposite orientation of the gradient (far right).

(B–D) Chemotaxis chamber assays exposing cells to (B) 0–200 μM 8-CPT-cAMP, (C) uniform 2 μM Sp-cAMPS, and (D) both. Leftward cell movement is indicated by a blue circle and rightward with a purple circle. Larger circles indicate a higher velocity in the specified direction. Scale bars, 100 μm.

*(legend continued on next page)*

cells simultaneously use a wide range of receptors to different attractants; neutrophils, for example, express hundreds of distinct receptors. This makes the prokaryotic scheme, in which repellents act by decreasing the number of activated molecules of one class of receptor, unfeasible; if a large number of different receptors each have a background activity, the overall effect of depressing one receptor type is small.

Despite this, negative chemotaxis clearly occurs and is important in normal physiology.[18,19] This paper examines the mechanisms that can allow this.

Recent work has focused on cell guidance by self-generated attractant gradients.[20–27] These are exceptionally dynamic, and the evolving ligand profiles are near-impossible to measure directly.[28] In contrast, the behavior of cells is readily observable and can be accurately predicted using computational models.[29] These models need not include complex receptor behavior (such as recycling, multimerization, and adaptation) to show strong predictive power. Here, we test the idea that different ligands can make complex and negative gradients by competing for simple, positively acting receptors. We combine computational modeling with experiments to show that molecules described as chemorepellents can work by interfering with positive signals, rather than via undiscovered negative signaling pathways.

## RESULTS

### Chemorepellents work by competing with positive agonist signals

8-CPT-cAMP (8- (4- Chlorophenylthio)adenosine-3',5'-cyclic monophosphate) has been described as a strong chemorepellent for Dictyostelium.[30,31] As an analog of cAMP, 8-CPT-cAMP is principally detected through the cAR1 receptor, which normally mediates a strongly attractive response to cAMP.[32] Because it is difficult to imagine this receptor acting both positively and negatively, we tested a different hypothesis—that it was acting as a receptor antagonist rather than a direct repellent. There is substantial evidence that 8-CPT-cAMP acts as a competitive inhibitor of cAMP's binding to cAR1. It binds to the receptor with a reasonable affinity[33] but requires concentrations at least 80× higher than would be expected from its affinity to induce chemotaxis or activate gene expression,[34] as well as actively blocking the effects of cAMP at lower concentrations,[34] and is thus considered a receptor antagonist.

If 8-CPT-cAMP acts as a competitive inhibitor, binding to the receptor but not activating it, it will not stimulate G-proteins and will give no directional cues on its own. In the presence of a stimulatory ligand, however, the 8-CPT-cAMP would compete for receptors; higher concentrations of 8-CPT-cAMP would keep more receptors in an inactive state. A gradient of 8-CPT-cAMP could therefore interact with uniform cAMP to create a reverse gradient of activated cAR1 receptors (represented in Figure 1A).

We tested this prediction using direct-view chemotaxis chambers,[35] which generate a defined gradient between two reservoirs (Figures 1B–1D; Video S1). Gradients of 8-CPT-cAMP do not give a steering response on their own (Figures 1B and measured in 1E) but strongly repel cells in the presence (Figures 1D and 1G) of homogeneous levels of a non-degradable cAMP analog, Sp-cAMPS (Adenosine-3',5'- cyclic monophosphorothioate, Sp-isomer), which strongly activates cAR1 but is not degraded.[36] Sp-cAMPS on its own gave no directional migration (Figures 1C and 1F).

Thus, the 8-CPT-cAMP does not repel cells directly but works very effectively through competition with an active ligand. This is not negative chemotaxis as usually understood—cells do not respond directly to the repellent—but it is remarkably effective (Video S1).

This implied that earlier results in which 8-CPT-cAMP was found as a direct chemorepellent,[31] worked through interaction with endogenous attractants. Dictyostelium cells complicate experimental results by secreting their own cAMP, which can be blocked using caffeine.[37] When we examined the chemotaxis of untreated cells using a micropipette, we found that wild-type cells were weakly repelled by 8-CPT-cAMP (Figures 1H and 1K), but we could never detect repulsion of caffeine-treated cells (Figures 1I and 1L). This suggests that cAMP produced by normal cells is essential for the observed repulsion. We therefore tested the effect of adding a homogeneous background of Sp-cAMPS. This fully rescued chemorepulsion, causing cells to migrate directly and efficiently away from the 8-CPT-cAMP released from a micropipette (Figures 1J and 1M; Video S2).

Taken together, these results demonstrate that chemorepulsion by 8-CPT-cAMP requires the presence of an attractant.

### Guidance uses receptor activity gradients, not attractant gradients

Our findings show that interacting ligands guide cells in unexpected ways. The system's complexity makes it hard to understand the underlying mechanisms intuitively. We therefore adapted our model of chemotaxis[25,38] to include steady-state competition for receptor sites between ligands (see Methods S1 for mathematics). In brief, the hybrid-agent-based model consists of a two-dimensional (2D) field describing concentrations of the chemoattractants, with individual cells as agents. All parameters (see Methods S1) are physiologically appropriate, with most experimentally measured. At each time point, the cells move a constant distance; each cell's direction is random, but biased by chemoattractant gradients measured by the difference in receptor occupancy between the front and back of the cell. The

(E and F) Rightward velocity across the experiments in (B)–(D). (E) 8-CPT-cAMP alone causes almost no movement. (F) Uniform Sp-cAMPS drives chemokinesis, not chemotaxis.

(G) Substantial movement away from 8-CPT-cAMP is apparent when both are included.

(H–J) NC4 cells stimulated by 10 mM 8-CPT-cAMP from a micropipette without caffeine (H), with caffeine (I), and with both caffeine and agonist background (2 μM Sp-cAMPS; J). Scale bars, 40 μm.

(K–M) Radial velocity toward the micropipette as a function of distance from it (K) without caffeine, (L) with caffeine, (M) with both caffeine and 2 μM Sp-cAMPS. Repulsion is slight (K), with caffeine treatment erasing it completely (L). Introduction of agonist makes the effect clear (M). Points show mean ± SE of technical replicates for cells in a representative experiment ($n \geq 30$, 48, and 28 respectively).

See also Videos S1 and S2.

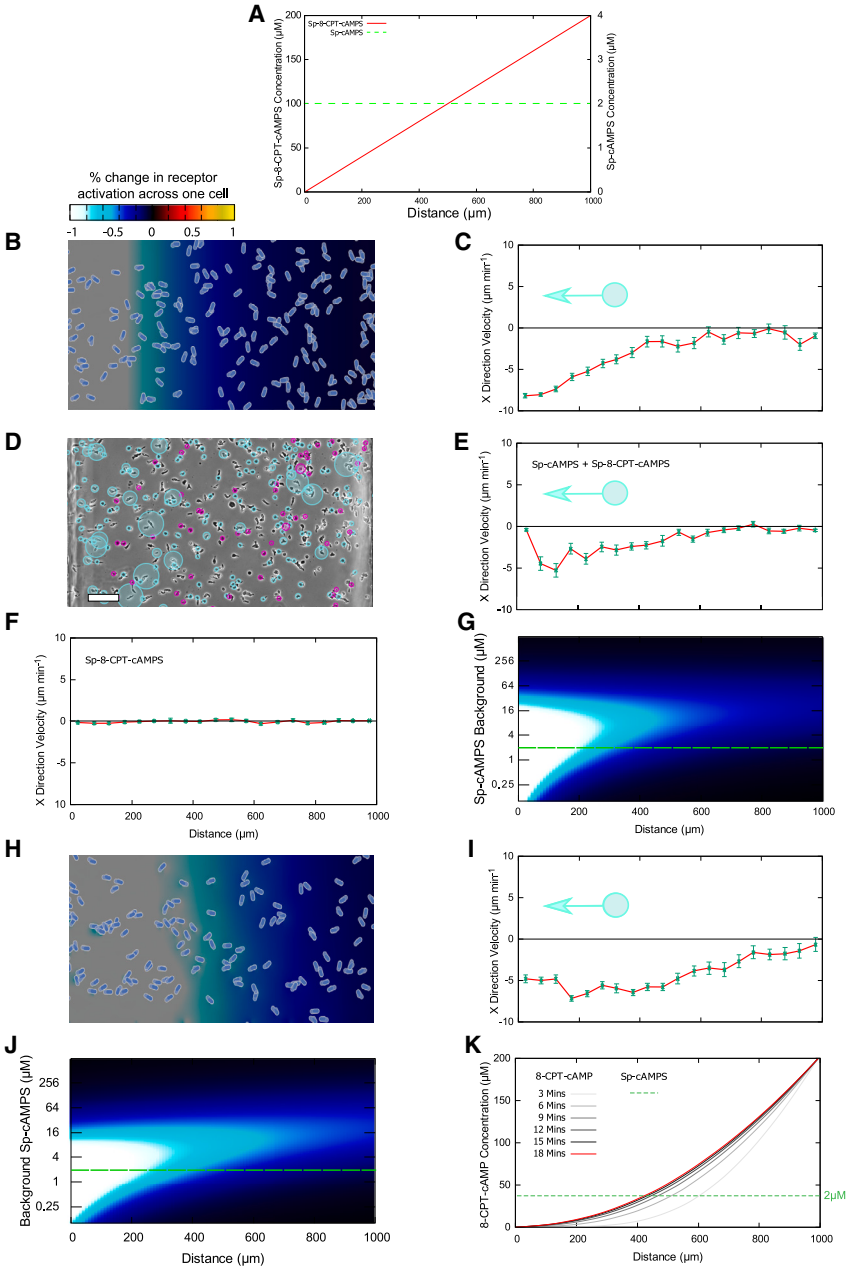


**Figure 2. Competitive chemorepulsion using degradable and non-degradable antagonists**

(A) Concentrations used in this figure. The non-degradable antagonist forms a linear steady state between the leftmost concentration of 0 and the rightmost concentration of 200 μM. A background agonist is included.

(B and C) Modeled chemotaxis under conditions described in (A). Colors show the local difference in receptor activity, with blue through white showing increasing leftward (i.e., repulsive) cues, and black to red to yellow showing stronger rightward (i.e., attractive) cues. (C) Quantitation, predicting repulsion at the left-hand side of the chamber.

(D and E) Experimental verification of modeled data. Cell tracking shows magenta circles for NC4 cells moving rightward and cyan circles for leftward movement. Scale bars, 100 μm.

(F) Velocity of real cells stimulated with Sp-8-CPT-cAMPS gradient alone.

(G) Heatmap showing differences in receptor activity, by position in the gradient (x axis) and background Sp-cAMPS concentration (y axis), assuming a linear 0–200 μM antagonist gradient. Higher concentrations of Sp-cAMPS improve chemorepulsion up to a point, beyond which Sp-cAMPS saturation inhibits guidance. Green dotted line indicates the concentration used in the experiments.

(H and I) Same as (B) and (C), but using antagonists that the cells degrade locally, leading to stronger, wider-ranging repulsion.

(J) As for (G), but for a degradable antagonist.

(K) Simulation of the evolution of a degradable antagonist gradient and the formation of a near-exponential gradient.

Green points in (C), (E), (F), and (I) show mean ± SE of technical replicates ($n \geq 53$, 23, 49, and 40, respectively) for cells at the indicated positions in a representative experiment.

steeper the gradient, the stronger the directional bias. After this, processes that change the attractant field are calculated. The model gives a faithful account of even complex processes like self-generated chemotaxis, so disagreements between experiment and model often reveal unexpected biology,[38] allowing us to test concepts around chemotaxis in detail.

We started without dynamic changes caused by ligand degradation. Simulations of a gradient of competitive antagonist with a background of non-degradable attractant (Figure 2A) predicted effective negative chemotaxis away from the antagonist. Interestingly, this effect is most pronounced at the bottom of the gradient and diminishes as the concentration of the repellent rises (Figures 2B and 2C). No appreciable repulsion is seen at the upper half of antagonist concentrations.

To reproduce this model in real cells, we required a ligand that combined being a full antagonist (such as 8-CPT-cAMP) with resistance to phosphodiesterase (such as Sp-cAMPS). Fortunately, these modifications are in different parts of the molecule, meaning that Sp-8-CPT-cAMPS (8- (4- Chlorophenylthio)adenosine- 3', 5'- cyclic monophosphorothioate, Sp- isomer) is both an antagonist and non-degradable. We found that experiments using a combination of Sp-8-CPT-cAMPS and Sp-cAMPS reproduce the behavior of the models almost perfectly (Figures 2D and 2E). A gradient of Sp-8-CPT-cAMPS alone gives no appreciable directionality across the whole bridge (Figure 2F), confirming that this molecule is a simple antagonist and that an agonist must be present for repulsion to be effective.

For a quantitative understanding of antagonistic repulsion, we built an analytical model of receptor occupancy across the whole of the chemotaxis chamber (see Methods S1). We used this to generate guidance heatmaps (Figure 2G) showing the effect of

different background attractant concentrations. This predicts an optimal background concentration of Sp-cAMPS of between 4 and 16 μM, about 4–16 times its $K_d$ for the receptor, cAR1 (Figure 2G). Below this, responses decline as the background agonist concentration drops and cell behavior therefore approaches the unsteered state. Predictions for different concentrations allowed us to refine our conceptual understanding. The agonist and antagonists actively compete for sites. Therefore, high agonist concentrations saturate receptor sites, diminishing the capacity of the antagonist to cause spatial bias. Low agonist concentrations are less effective because there is less active signal to outcompete.

The non-degradable inhibitor gave a less robust response across a smaller proportion of the bridge (see Figures 1D and 1G). This was surprising, as we had expected degradation to mute the repellent's effect. We tested this using simulations, which replicated both the enhanced strength and the range of a degradable chemorepellent (Figures 2H–2K). The simulation revealed that the interaction of diffusion and degradation creates an approximately exponential gradient across the chamber (Figure 2L), exposing cells to a steeper gradient of receptor inhibition. Thus, cells can obtain more information from chemorepellents by degrading them, just as they can with chemoattractants.[26]

### Antagonist gradients can reverse positive cues

We tested whether two gradients could interact together to give repulsion. Simulation of combined agonist and antagonist gradients (Figures 3A and 3B) predicted a negative response (Figures 3C–3F), as long as the agonist started at a significant level (Figure 3B). For both attractant alone and the combination, chemotaxis was clearest at the lower end of the gradient (Figures 3E and 3F). Real cells behaved as the model predicted (Figures 3G–3J). The dose response of this repulsion is complex—agonist and antagonist gradients in the same direction can be repulsive, but only if the growth in antagonist is enough to overcome the attractive signal.

In conclusion, shallow agonist gradients are able to combine with steeper antagonist gradients to steer cells negatively. Above a critical steepness, at which the two balance out, the guidance direction reverses (Figure 3K).

### Interactions between degradable and non-degradable attractants and repellents

Because cells can increase the strength and range of negative chemotaxis by locally degrading the antagonist (Figures 2G and 2J), we examined the interactions between degradable attractants and repellents. Cells completely degrade low concentrations of cAMP signal, which means that they cannot perceive the interfering gradient. However, by adding a small amount of non-degradable Sp-cAMPS, we maintained a detectable signal (Figure 4A). This allowed experiments with a near-exponential gradient across most of the chamber, while still maintaining competition between antagonist and agonist. Simulations of this setup made a striking prediction—the cells diverged at the midpoint of the chamber, with those in the left half moving left and those in the right half moving right (Figures 4B and 4C), opening up a gap in the center. Real cells replicated this behavior (Figures 4D and 4E; Video S3), again showing the accuracy of the simulations. Plotting simulated receptor occupancy shows that this combination allows an exponential gradient of cAMP to dominate the right half of the chamber (Figure 4F), climbing far faster than the antagonist gradient. In contrast, the cAMP was at near zero levels on the left-hand side of the chamber, so the gradient was too shallow to affect the repellent effect of the other ligands.

This experimental condition—in which the cells change direction depending on their position in the gradient—is very unusual (Figure 4F). In a simple attractant gradient, the guidance cues are stronger at the low end, but at higher concentrations the difference between front and rear becomes less and they lose their sense of direction (for example, Figures 3G and 3I). The behavioral turning point is neither a source of attractant nor of antagonist, but the result of a complex competition between different ligands.

We also tested whether the opposite was true, and degradable antagonists could lead to convergence in the middle of the gradient. Simulations predicted that degradable antagonist gradients could be shallow enough at their lower ends to be outcompeted by a moderate linear agonist gradient. At the same time, higher concentrations and the exponential nature of a degradable antagonist at the high end can overwhelm the linear agonist gradient (Figure 5A). This leads to a striking maximum of receptor activity in the middle of the chamber, which causes cells from everywhere in the bridge to converge (Figures 5B and 5C; Video S4). Experiments with real cells again followed the simulations accurately (Figures 5D and 5E). One difference was particularly informative—real cells in antagonists ceased making protrusions and stopped moving, rather than continuing with the random movement as we see in unstimulated cells (see Video S4). The principal result is that competition between ligands can direct cells to positions that are different from the source of either ligand, which depends on the $K_d$ of the antagonist relative to the agonist (Figure 5F).

### Complex outcomes from mixed signals: Chemorepulsion by competing gradients

Many physiologically important examples of chemotaxis are remarkably complex. For example, there are >40 chemokines, transduced by around 20 receptors; each receptor may detect many chemokines, and some chemokines activate different receptors to different degrees. Furthermore, under physiological conditions many of these chemokines are present together. This leads to a wide range of possible interactions that exceeds an experimenter's ability to explore them. Because our chemotaxis model had consistently given dependable results, we used it to explore the possible effects of mixing different ligands.

One set of simulations gave particularly counterintuitive results—competition between different ligands binding to the same receptor. Receptors are normally in an "inactive" state. When they are in an "active" state, they bind to G-proteins and cause effects inside the cell. When a perfect receptor binds to its ligand, it always changes from inactive to active. However, real-life receptors are not perfect; ligand binding only activates a fraction of them. This is termed the efficacy, and it differentiates an agonist from an antagonist. Strong agonists, for example, cAMP, have an efficacy close to 1, whereas antagonists like

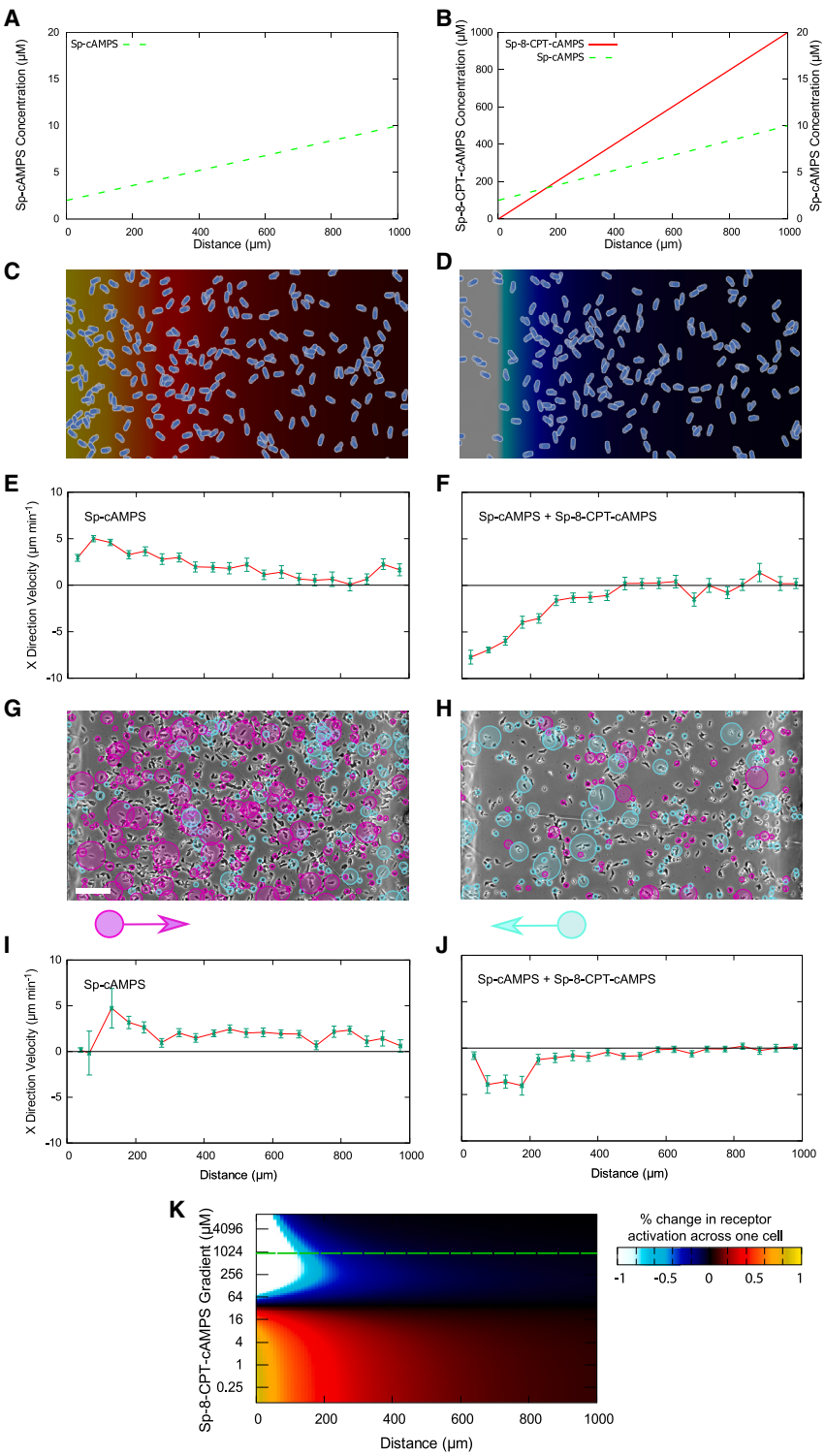


**Figure 3. Interference between colinear agonist and antagonist gradients**

(A and B) Diagrams of the conditions in the figure, a 2- to 10-μM agonist (Sp-cAMPS) gradient alone (A), and a 0- to 1-mM antagonist (Sp-8-CPT-cAMPS) gradient (B).

(C–F) Modeled chemotaxis under conditions shown in (A) and (B). Agonist alone drives positive chemotaxis (C), but overall guidance is repellent when the antagonist is introduced (D). (E and F) Quantitative analysis of rightward velocity.

(G–J) Experimental validation of (C)–(F). Tracking of NC4 cells shows the attractive (G) and repellent (H) regimes, with the rightward velocity quantified in a representative experiment (I and J). Scale bars, 100 μm.

(K) Heatmap showing difference in the proportion of activated receptors between the front and the back of cells, by position in the gradient (x axis) and steepness of the non-degradable antagonist gradient (y axis), assuming the presence of the linear agonist gradient shown in (A) and (B). Shallow antagonist gradients leave the agonist able to guide cells toward the right, but steeper gradients reverse the direction of guidance. Green dotted line shows the conditions used in the rest of the figure. Green points in (E), (F), (I), and (J) show mean ± SE of technical replicates ($n \geq 53$, 33, 36, and 46) for cells at the indicated positions in a representative experiment.

8-CPT-cAMP have an efficacy of effectively zero. Ligands with intermediate efficacies are partial agonists. They appear to be weaker attractants, but because they still activate some receptors they can still generate positive guidance cues.

We simulated three conditions: a gradient of agonists, a gradient of partial agonists, and both gradients expressed together (Figures 6A–6I). In Dictyostelium, the cAMP analog Rp-cAMPS ((Adenosine-3',5'- cyclic monophosphorothioate, Rp-isomer) is a partial agonist, so we simulated the interaction between Sp-cAMPS and Rp-cAMPS.

Cells chemotax up simple gradients of either the partial agonist Rp-cAMPS (Figures 6D and 6G) or the efficient agonist Sp-cAMPS (Figures 6E and 6H). When these gradients are superimposed, the simulations make an extraordinary prediction. Not only do the two gradients not reinforce one another but together they also actively repel cells (Figures 6F, 6I, and 6J).

Mathematical analysis indicates that a second competing agonist cannot reinforce signals if the first agonist gradient is steep. The switch to repulsive behavior requires two things—a background of the first attractant throughout the gradients and lower efficacy for the second attractant (Figure 6L shows the effects of different efficacies—we estimate the efficacy of Rp-cAMPS to be around 0.3, meaning that of 10 receptors bound to Rp-cAMPS, 3 will become activated). We examined the results we would expect from different gradient steepnesses of a partial agonist with this efficacy (Figure 6K). Shallower gradients leave the full agonist able to dominate.

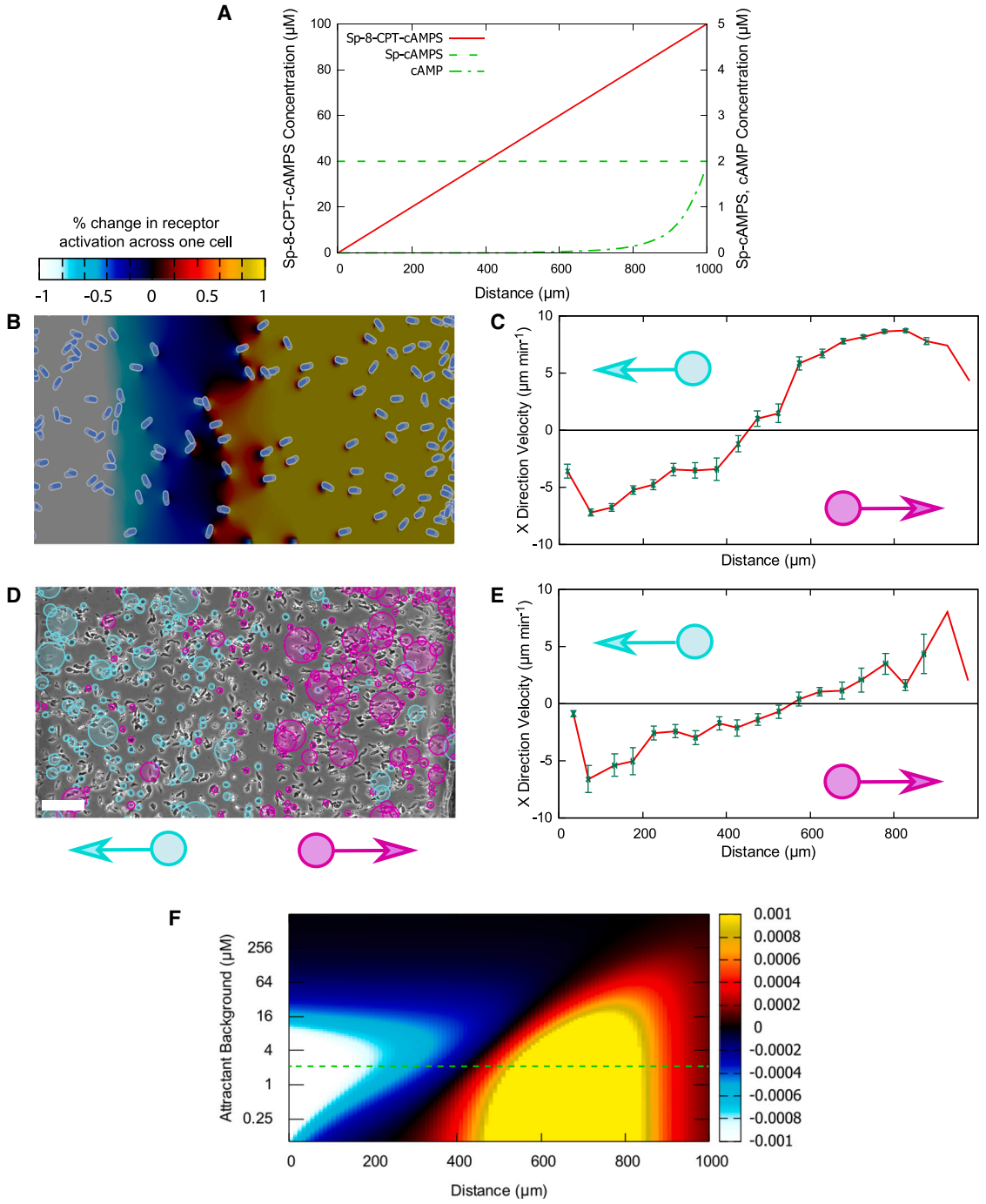


**Figure 4. Divergent guidance from 3-ligand interaction with a degradable agonist**

(A) Diagram of conditions used. A linear gradient of 0–100 μM Sp-8-CPT-cAMPS antagonizes a 0- to 5-μM (initially, before degradation) cAMP gradient, which becomes exponential due to attractant degradation. A 2-μM background of Sp-cAMPS maintains receptor activation.

(B) Modeled chemotaxis, with background color showing receptor activity difference across the cell. Expected receptor activity has a minimum in the middle of the chamber, leading cells to either side.

(C) Quantification of velocity in (B).

(D and E) Experimental verification of the predictions in (B) and (C), with cells moving leftward highlighted in cyan and rightward in purple. Scale bars, 100 μm.

(F) Heatmap of the calculated difference in proportion of receptor activity across cells for the conditions described in (A), with antagonist background concentration varying on the y axis. The black zone in the middle of the map shows the midpoint where cell behavior diverges. Green points in (C) and (E) show mean ± SE of technical repeats ($n \geq 23$ and 32) for cells at the indicated positions of a representative experiment (E) or 3 repeated simulations (C).

See also Video S3.

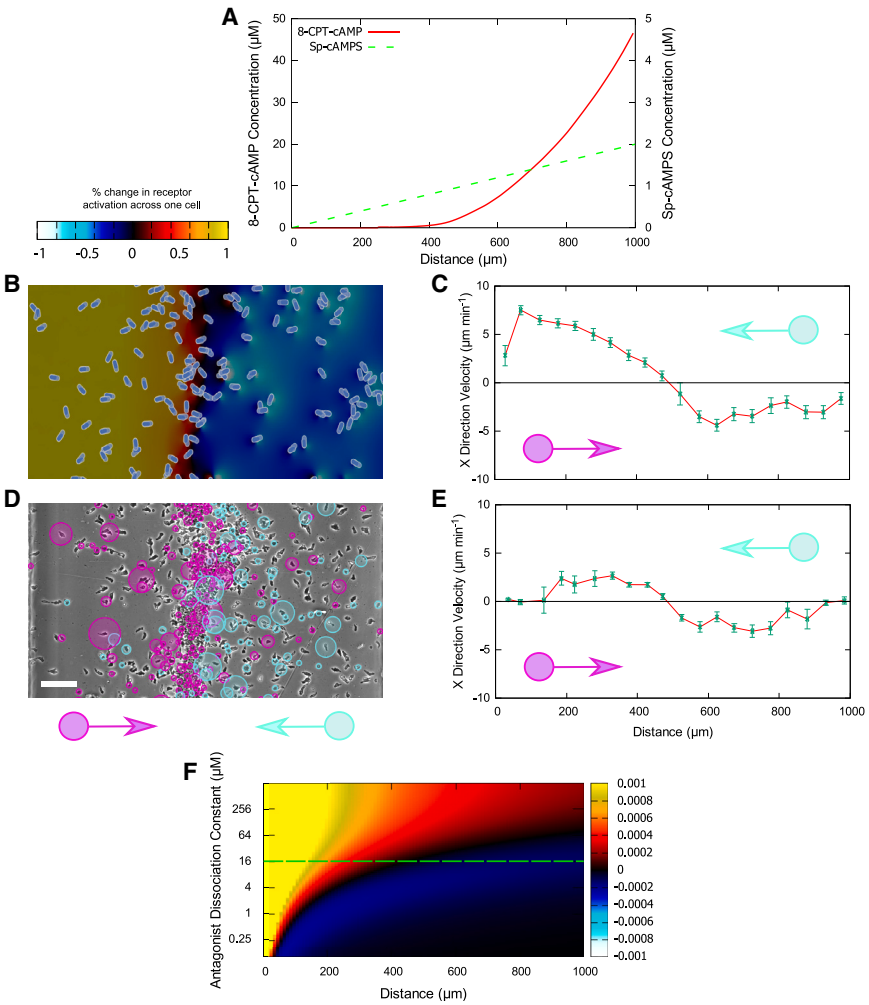


**Figure 5. Convergent guidance from stable agonist and degradable antagonist interference**

(A) Diagram of conditions used. A linear gradient of 0- to 2 μM-Sp-cAMPS provides an agonist stimulus against which a 0–80 μM 8-CPT-cAMP gradient interferes. Cell degradation of the latter makes an exponential shape at equilibrium.

(B) Modeled chemotaxis, with background color showing receptor activity difference across the cell. Cells converge on a central point.

(C) Quantification of rightward velocity in (B).

(D and E) Experimental verification of predictions in (B) and (C), with cells moving leftward highlighted in cyan and rightward in purple. Scale bars, 100 μm.

(F) Heatmap of calculated receptor activity gradient for conditions described in (A), with antagonist $K_d$ varying on the y axis. The black zone in the middle of the map shows the midpoint where cell behavior converges. Green points in (C) and (E) show mean ± SE ($n \geq 23$ and 13) for cells at the indicated positions, in 3 experiments (C) or representative experiment (E).

See also Video S4.

Above a critical steepness at which the two signals cancel one another out (around 7 μM, in this case) guidance cues become repellent.

These results from the model were completely counterintuitive; to our knowledge, nothing like this has been observed previously. We therefore used this as a test of the computational model's usefulness. The conditions that work best are almost impossible to guess from first principles, but the models illuminate the range of conditions that can work. Experiments with real cells, using concentrations suggested by the models, accurately replicated the remarkable result (Figures 6M–6R; Video S5)—Sp-cAMPS gradients cause positive chemotaxis, Rp-cAMPS gradients cause positive chemotaxis, but when the exact same two gradients are combined, they become repulsive.

This confirms two important points. First, our mathematical model of chemotaxis is a precise enough tool to explore the outcomes of multiple, complex conditions and faithfully predict cells' behavior; this is important when there are so many possible experiments, and it allows a much better mechanistic understanding. Second, very unexpectedly, competition between two attractant ligands for the same receptors can give negative chemotaxis.

## DISCUSSION

Chemotaxis is fundamentally important to normal eukaryotic biology, and thus widely studied. Many important cases—for example, neutrophils responding to infections by chemotaxing toward chemokines—involve many different ligands competing for a smaller pool of receptors. For example, the CXCR2 receptor binds to CXCLs 1, 2, 3, 5, and 8; all are physiologically important.[1] These ligands' chemotactic effects are generally studied individually; we do not know of experiments studying chemotaxis combinations of different CXCLs. This, combined with the need for mathematical modeling to dissect the interactions, means that the role of competition in negative chemotaxis has not been seen previously. The data we have described show that this competition is fundamentally important to chemotaxis *in vivo*, and understanding it will yield important—if counterintuitive—results.

We have shown how GPCRs can mediate negative chemotaxis without invoking any currently unknown molecular mechanisms. As this relies on competition between ligands, further study into systems with apparent GPCR-mediated chemorepulsion will need to account for competing signals that communicate through the same receptor. Crucially, the findings are not limited to GPCRs: the same mechanisms will work for any receptor type. For example, Robo-mediated guidance is known to involve both full-length Slit and Slit-N,[39] suggesting competitive rather than direct repulsion, and the same is true for the pairing of semaphorins and Slit-C with Plexin-1A.[40]

While systems with only one or two known signals might become straightforward when viewed in the context of this work, others are more complex. The chemokine system, for

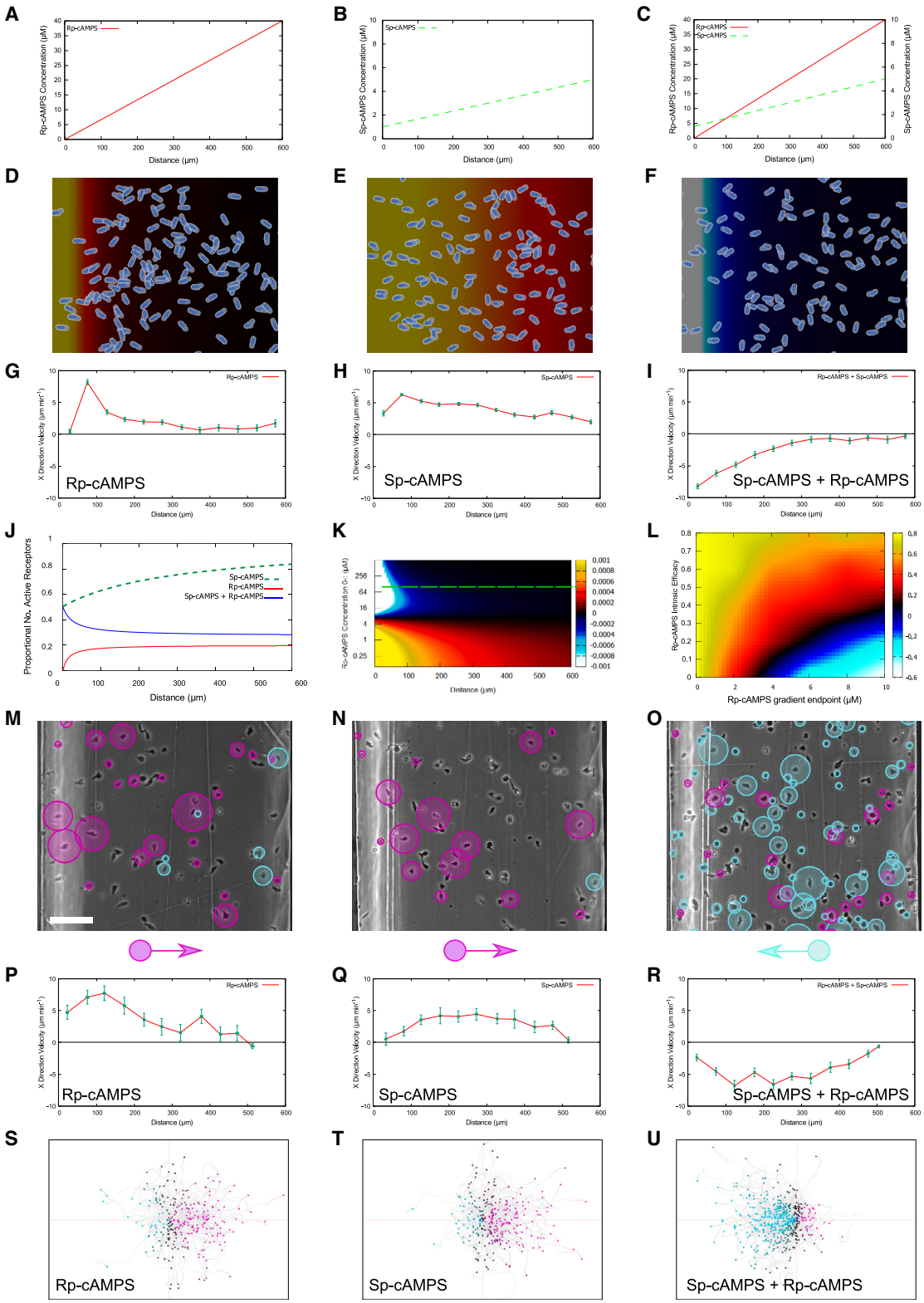


**Figure 6. Combined attractant gradients cause repulsion**

(A–C) Diagrams of the conditions, a 0–40 μM gradient of the partial agonist Rp-cAMPS (A), a 1–5 μM gradient of the agonist (Sp-cAMPS) (B), and both together (C). (D–F) Modeled chemotaxis in conditions (A)–(C). Both the partial agonist (D) and the agonist (E) drive positive chemotaxis, but cells are repelled when both gradients are present (F).

*(legend continued on next page)*

example, involves complex, promiscuous interactions between receptors and ligands, and an array of ligand modifications that change the $K_d$ and efficacy for different receptor-ligand interactions. This has been described as "redundancy,"[41] but our finding that competition between ligands gives complex effects (Figure 6) disagrees. It is more likely that a healthy immune system places chemokines at a series of tipping points, ready to mediate attraction or repulsion in specific cell types at different times and places. This would explain the high failure rate of chemokine receptor targeting drugs; understanding it would improve the development of new ones.

This also emphasizes the importance of studying simplified systems. Our studies succeeded because we could eliminate the breakdown of attractants and repellents by cells (using Sp-modifications) and prevent them from secreting their own attractants (using caffeine and by knocking out adenylyl cyclase). Without this, even Dictyostelium is too complex to understand quantitatively, even though it essentially responds to only one chemoattractant. Immune cells chemotax to multiple signals, using many receptors, many of which (for example, LTB4[42]) are autocrine.

More generally, seeing chemotaxis from the cell's view (as a simple spatial bias in receptor activation) rather than the experimenter's (multiple, separate attractant gradients) introduces mechanisms of control that apply in any context. Our investigation into 8-CPT-cAMP shows that the strength of an effective repellent is tuned by the concentration of a ubiquitous agonist and turned off entirely without an agonist. We show that the inclusion of a competitive antagonist can turn an attractive guidance cue into a repellent one (Figure 3). This would be an excellent mechanism for resolving inflammation. After some threshold is passed, an attractive signal could be competed out by a different agonist, reversing the directional instruction.

We have shown many ways in which chemotaxis is complex and counterintuitive. Attractant degradation[25] can be vital to long-range guidance, and local topology can interact with guidance cues, even as far as to lead cells away from major attractant sources.[38] We now add ligand competition to the complex mechanisms that guide cells. Our examples of ligand competition use effectively 1D environments—the cell's chemotactic stimuli are defined simply by how far across the chamber they are. If we extend this into 2D and 3D, competition will be even more dynamic and unexpected. Understanding this will require extensive mathematical and computational modeling, combined iteratively with experimental measurements. The counterintuitive nature of these questions means that we could not design informative experiments without computational simulations to test the implications of our current understanding. In any case, it is increasingly clear that real guidance cues emerge from the interactions of several signals, and they must be considered together to be understood.

## STAR★METHODS

Detailed methods are provided in the online version of this paper and include the following:

- KEY RESOURCES TABLE
- RESOURCE AVAILABILITY
  - Lead contact
  - Materials availability
  - Data and code availability
- EXPERIMENTAL MODEL AND SUBJECT DETAILS
- METHOD DETAILS
  - Models
  - Gene knockouts
  - Assay preparation
  - Chemotaxis chamber assays
  - Micropipette Assays
  - Simulations
  - Wild-Type NC4 Bridge Chamber Assays
- QUANTIFICATION AND STATISTICAL ANALYSIS

## SUPPLEMENTAL INFORMATION

Supplemental information can be found online at https://doi.org/10.1016/j.cub.2023.03.006.

## ACKNOWLEDGMENTS

We are grateful to Cancer Research UK (CRUK) for core funding to the CRUK Beatson Institute (A31287) and to R.H.I. (A19257), and to the Wellcome Trust for grant 221786/Z/20/Z to R.H.I.

## AUTHOR CONTRIBUTIONS

Conceptualization, A.D., L.T., and R.H.I.; experimental design, A.D. and P.A.T.; experimental investigation, A.D. and P.I.P.; simulations, A.D. and L.T.; writing, A.D., L.T., and R.H.I.; supervision, L.T., P.A.T., and R.H.I.; funding acquisition, R.H.I.

## DECLARATION OF INTERESTS

The authors declare no competing interests.

(G–I) Rightward velocity quantified for (D)–(F).
(J) Computed fraction of receptors that are activated across the bridge of the chamber.
(K) Heatmap of the receptor activity differences across the chamber when varying the steepness of the partial agonist gradient, assuming its efficacy is 0.3 and presence of the linear agonist gradient shown in (B) and (C). Shallow partial agonist gradients allow the full agonist to drive positive chemotaxis, but steeper gradients switch the cues to repellent ones. The green dotted line shows the predicted behavior for the gradient used in the rest of the figure.
(L) Heatmap showing the proportion of simulated cells that show positive (warm colors) or negative (cold colors) chemotaxis, as the efficacy and final concentration of the imperfect agonist are varied. The linear attractant gradient illustrated in (B) competes against the linear imperfect inhibitor. Measurements were made over 40 min of simulated chemotaxis.
(M–U) Experimental validation of (D)–(I). Tracked *aca*A$^-$ cells show chemotaxis to both Rp-cAMPS and Sp-cAMPS individually (M) and (N), and repulsion when both are present (O). Scale bars, 100 μm.
Green points in (G)–(I), (M), (N), and (O) show mean ± SE ($n \geq 68, 80, 48, 8, 3$, and 19) for cells at the indicated positions, in 3 simulations (G–I) or a representative experiment (M–O).
See also Video S5.

Received: December 6, 2022
Revised: February 24, 2023
Accepted: March 3, 2023
Published: March 30, 2023

## REFERENCES

1. Tharp, W.G., Yadav, R., Irimia, D., Upadhyaya, A., Samadani, A., Hurtado, O., Liu, S.Y., Munisamy, S., Brainard, D.M., Mahon, M.J., et al. (2006). Neutrophil chemorepulsion in defined interleukin-8 gradients in vitro and in vivo. J. Leukoc. Biol. *79*, 539–554.
2. Pasquale, E. (2000). Neurobiology. Turning attraction into repulsion. Science *289*, 1308–1310.
3. Colom, B., Bodkin, J.V., Beyrau, M., Woodfin, A., Ody, C., Rourke, C., Chavakis, T., Brohi, K., Imhof, B.A., and Nourshargh, S. (2015). Leukotriene B4-neutrophil elastase axis drives neutrophil reverse transendothelial cell migration in vivo. Immunity *42*, 1075–1086.
4. Consalvo, K.M., Kirolos, S.A., Sestak, C.E., and Gomer, R.H. (2022). Sex-based differences in human neutrophil chemorepulsion. J. Immunol. *209*, 354–367.
5. Zaki, M., Andrew, N., and Insall, R.H. (2006). Entamoeba histolytica cell movement: a central role for self-generated chemokines and chemorepellents. Proc. Natl. Acad. Sci. USA *103*, 18751–18756.
6. Jongsma, M., Matas-Rico, E., Rzadkowski, A., Jalink, K., and Moolenaar, W.H. (2011). LPA is a chemorepellent for B16 melanoma cells: action through the cAMP-elevating LPA5 receptor. PLoS One *6*, e29260.
7. Sakai, J.A., and Halloran, M.C. (2006). Semaphorin 3d guides laterality of retinal ganglion cell projections in zebrafish. Development *133*, 1035–1044.
8. Fiore, R., Rahim, B., Christoffels, V.M., Moorman, A.F., and Püschel, A.W. (2005). Inactivation of the Sema5a gene results in embryonic lethality and defective remodeling of the cranial vascular system. Mol. Cell. Biol. *25*, 2310–2319.
9. Holmes, G.R., Anderson, S.R., Dixon, G., Robertson, A.L., Reyes-Aldasoro, C.C., Billings, S.A., Renshaw, S.A., and Kadirkamanathan, V. (2012). Repelled from the wound, or randomly dispersed? Reverse migration behavior of neutrophils characterized by dynamic modelling. J. R. Soc. Interface *9*, 3229–3239.
10. Tso, W.W., and Adler, J. (1974). Negative chemotaxis in Escherichia coli. J. Bacteriol. *118*, 560–576.
11. Toews, M.L., Goy, M.F., Springer, M.S., and Adler, J. (1979). Attractants and repellents control demethylation of methylated chemotaxis proteins in Escherichia coli. Proc. Natl. Acad. Sci. USA *76*, 5544–5548.
12. Devreotes, P.N., and Zigmond, S.H. (1988). Chemotaxis in eukaryotic cells: a focus on leukocytes and Dictyostelium. Annu. Rev. Cell Biol. *4*, 649–686.
13. Gerisch, G., and Keller, H.U. (1981). Chemotactic reorientation of granulocytes stimulated with micropipettes containing fMet-Leu-Phe. J. Cell Sci. *52*, 1–10.
14. Insall, R., and Andrew, N. (2007). Chemotaxis in Dictyostelium: how to walk straight using parallel pathways. Curr. Opin. Microbiol. *10*, 578–581.
15. Neptune, E.R., and Bourne, H.R. (1997). Receptors induce chemotaxis by releasing the betagamma subunit of Gi, not by activating Gq or Gs. Proc. Natl. Acad. Sci. USA *94*, 14489–14494.
16. Neptune, E.R., Iiri, T., and Bourne, H.R. (1999). Galphai is not required for chemotaxis mediated by Gi-coupled receptors. J. Biol. Chem. *274*, 2824–2828.
17. Malet-Engra, G., Yu, W., Oldani, A., Rey-Barroso, J., Gov, N.S., Scita, G., and Dupré, L. (2015). Collective cell motility promotes chemotactic prowess and resistance to chemorepulsion. Curr. Biol. *25*, 242–250.
18. Nourshargh, S., Renshaw, S.A., Imhof, B.A., Reverse Migration of Neutrophils, Nourshargh, S., Renshaw, S.A., and Imhof, B.A. (2016). Reverse Migration of Neutrophils: Where, When, How, and Why? Trends Immunol. *37*, 273–286.
19. Robertson, A.L., Holmes, G.R., Bojarczuk, A.N., Burgon, J., Loynes, C.A., Chimen, M., Sawtell, A.K., Hamza, B., Willson, J., Walmsley, S.R., et al. (2014). A zebrafish compound screen reveals modulation of neutrophil reverse migration as an anti-inflammatory mechanism. Sci. Transl. Med. *6*, 225ra29.
20. Dalle Nogare, D., and Chitnis, A.B. (2017). A framework for understanding morphogenesis and migration of the zebrafish posterior Lateral Line primordium. Mech. Dev. *148*, 69–78.
21. Donà, E., Barry, J.D., Valentin, G., Quirin, C., Khmelinskii, A., Kunze, A., Durdu, S., Newton, L.R., Fernandez-Minan, A., Huber, W., et al. (2013). Directional tissue migration through a self-generated chemokine gradient. Nature *503*, 285–289.
22. Insall, R.H., Paschke, P., and Tweedy, L. (2022). Steering yourself by the bootstraps: how cells create their own gradients for chemotaxis. Trends Cell Biol. *32*, 585–596.
23. Muinonen-Martin, A.J., Susanto, O., Zhang, Q., Smethurst, E., Faller, W.J., Veltman, D.M., Kalna, G., Lindsay, C., Bennett, D.C., Sansom, O.J., et al. (2014). Melanoma cells break down LPA to establish local gradients that drive chemotactic dispersal. PLoS Biol. *12*, e1001966.
24. Shellard, A., and Mayor, R. (2021). Collective durotaxis along a self-generated stiffness gradient in vivo. Nature *600*, 690–694.
25. Tweedy, L., Knecht, D.A., Mackay, G.M., and Insall, R.H. (2016). Self-generated chemoattractant gradients: attractant depletion extends the range and robustness of chemotaxis. PLoS Biol. *14*, e1002404.
26. Tweedy, L., and Insall, R.H. (2020). Self-generated gradients yield exceptionally robust steering cues. Front. Cell Dev. Biol. *8*, 133.
27. Venkiteswaran, G., Lewellis, S.W., Wang, J., Reynolds, E., Nicholson, C., and Knaut, H. (2013). Generation and dynamics of an endogenous, self-generated signaling gradient across a migrating tissue. Cell *155*, 674–687.
28. Tweedy, L., Susanto, O., and Insall, R.H. (2016). Self-generated chemotactic gradients-cells steering themselves. Curr. Opin. Cell Biol. *42*, 46–51.
29. Neilson, M.P., Veltman, D.M., van Haastert, P.J., Webb, S.D., Mackenzie, J.A., and Insall, R.H. (2011). Chemotaxis: a feedback-based computational model robustly predicts multiple aspects of real cell behavior. PLoS Biol. *9*, e1000618.
30. Keizer-Gunnink, I., Kortholt, A., and Van Haastert, P.J. (2007). Chemoattractants and chemorepellents act by inducing opposite polarity in phospholipase C and PI3-kinase signaling. J. Cell Biol. *177*, 579–585.
31. Cramer, L.P., Kay, R.R., and Zatulovskiy, E. (2018). Repellent and attractant guidance cues initiate cell migration by distinct rear-driven and front-driven cytoskeletal mechanisms. Curr. Biol. *28*, 995–1004.e3.
32. Pupillo, M., Insall, R., Pitt, G.S., and Devreotes, P.N. (1992). Multiple cyclic AMP receptors are linked to adenylyl cyclase in Dictyostelium. Mol. Biol. Cell *3*, 1229–1234.
33. van Ments-Cohen, M., Genieser, H.G., Jastorff, B., Van Haastert, P.J., and Schaap, P. (1991). Kinetics and nucleotide specificity of a surface cAMP binding site in Dictyostelium discoideum, which is not down-regulated by cAMP. FEMS Microbiol. Lett. *66*, 9–14.
34. Peters, D.J., Bominaar, A.A., Snaar-Jagalska, B.E., Brandt, R., Van Haastert, P.J., Ceccarelli, A., Williams, J.G., and Schaap, P. (1991). Selective induction of gene expression and second-messenger accumulation in Dictyostelium discoideum by the partial chemotactic antagonist 8-p-chlorophenylthioadenosine 3′,5′-cyclic monophosphate. Proc. Natl. Acad. Sci. USA *88*, 9219–9223.
35. Muinonen-Martin, A.J., Veltman, D.M., Kalna, G., and Insall, R.H. (2010). An improved chamber for direct visualisation of chemotaxis. PLoS One *5*, e15309.
36. Theibert, A., Palmisano, M., Jastorff, B., and Devreotes, P. (1986). The specificity of the cAMP receptor mediating activation of adenylate cyclase in Dictyostelium discoideum. Dev. Biol. *114*, 529–533.

37. Theibert, A., and Devreotes, P.N. (1983). Cyclic 3′, 5′-AMP relay in Dictyostelium discoideum: adaptation is independent of activation of adenylate cyclase. J. Cell Biol. *97*, 173–177.

38. Tweedy, L., Thomason, P.A., Paschke, P.I., Martin, K., Machesky, L.M., Zagnoni, M., and Insall, R.H. (2020). Seeing around corners: cells solve mazes and respond at a distance using attractant breakdown. Science *369*, eaay9792.

39. Bhat, K.M. (2017). Post-guidance signaling by extracellular matrix-associated Slit/Slit-N maintains fasciculation and position of axon tracts in the nerve cord. PLoS Genet. *13*, e1007094.

40. Delloye-Bourgeois, C., Jacquier, A., Charoy, C., Reynaud, F., Nawabi, H., Thoinet, K., Kindbeiter, K., Yoshida, Y., Zagar, Y., Kong, Y., et al. (2015). PlexinA1 is a new Slit receptor and mediates axon guidance function of Slit C-terminal fragments. Nat. Neurosci. *18*, 36–45.

41. Wolf, M., Albrecht, S., and Märki, C. (2008). Proteolytic processing of chemokines: implications in physiological and pathological conditions. Int. J. Biochem. Cell Biol. *40*, 1185–1198.

42. Lämmermann, T., Afonso, P.V., Angermann, B.R., Wang, J.M., Kastenmüller, W., Parent, C.A., and Germain, R.N. (2013). Neutrophil swarms require LTB4 and integrins at sites of cell death in vivo. Nature *498*, 371–375.

43. Paschke, P., Knecht, D.A., Silale, A., Traynor, D., Williams, T.D., Thomason, P.A., Insall, R.H., Chubb, J.R., Kay, R.R., and Veltman, D.M. (2018). Rapid and efficient genetic engineering of both wild type and axenic strains of Dictyostelium discoideum. PLoS One *13*, e0196809.

44. Muinonen-Martin, A.J., Knecht, D.A., Veltman, D.M., Thomason, P.A., Kalna, G., and Insall, R.H. (2013). Measuring chemotaxis using direct visualization microscope chambers. Methods Mol. Biol. *1046*, 307–321.

## STAR★METHODS

### KEY RESOURCES TABLE

| REAGENT or RESOURCE | SOURCE | IDENTIFIER |
|---|---|---|
| Chemicals, Peptides, and Recombinant Proteins | | |
| SM agar | formedium.com | SM |
| Caffeine | Sigma | C0750 |
| cyclic AMP | Sigma | A3262 |
| Sp-cAMPS | BioLog Life Sciences Institute | A003S |
| Rp-cAMPS | BioLog Life Sciences Institute | A002T |
| 8-CPT-cAMP | BioLog Life Sciences Institute | C010 |
| Sp-8-CPT-cAMPS | BioLog Life Sciences Institute | C012 |
| Experimental Models: Organisms/Strains | | |
| NC4 aca- | This work | sPI844 |
| Software and Algorithms | | |
| Self-generated gradient model | Tweedy et al., 2020[38] | GitHub: https://github.com/ltweedy/MazeNavigation |

### RESOURCE AVAILABILITY

#### Lead contact

Further information and requests for resources and reagents should be directed to and will be fulfilled by the lead contact, Prof. Robert Insall (robert@chemotaxis.org)

#### Materials availability

The NC4 *aca*A- line will be deposited in the Dictyostelium Stock Center (dictybase.org)

#### Data and code availability

- All data reported in this paper will be shared by the lead contact upon request.
- All original code has been deposited at Github and is publicly available as of the date of publication. Code is available at https://github.com/ltweedy/MazeNavigation
- Any additional information required to reanalyze the data reported in this paper is available from the lead contact upon request.

### EXPERIMENTAL MODEL AND SUBJECT DETAILS

Dictyostelium cells were originally obtained from the Dictyostelium stock center. Two *Dictyostelium* strains were utilised in this paper, wild type NC4 (WT) and NC4 adenylyl cyclase knockouts (*aca*A$^-$). Both were grown on *Klebsiella aerogenes*, passaged once weekly. Lawns of bacteria on SM agar plates (formedium.com) were inoculated with a small amount of bacterial stock from -80° stock. When this had grown into a colony, a streak of about 5 x $10^5$ cells was used to start a growth plate together with fresh Klebsiella. Plates were kept at 22°C for 48h then Dictyostelium were harvested and washed free of bacteria. The *K. aerogenes* was also passaged once weekly. Fresh stocks of bacteria and both NC4 strains were retrieved from -80°C once per month.

### METHOD DETAILS

#### Models

Cell migration was simulated as described in the text using a hybrid agent-based and finite-elemnt diffusion model as described in Methods S1.

### Gene knockouts

The *aca*A- cells were generated by inserting a hygromycin resistance cassette into plasmid sPI844 containing the the locus of *acaA* gene (4500 bp), replacing about 2500 bp (800 bp to 3300 bp) of its sequence. The used recombination arms span from -300 bp to 800 bp and 3300 to 4500 bp of the genomic sequence. This was electroporated into bacterially-grown NC4 Schaap cells using the method and parameters described in Paschke et al.[43] Clones were isolated on SM agar plates and screened using PCR.

### Assay preparation

For both WT and *aca*A$^-$ strains, experiments were set up two days in advance by growing cells on four different agar plates at varying cell densities. On the day of the experiment the plate with the most consumed bacteria and least sign of further starvation was harvested, and the cells washed in KK2 buffer (K phosphate pH6.2), with added 2mM $MgCl_2$ and 0.1mM $CaCl_2$ (to give KK2MC) three times at 1300 rpm for 3 minutes.

For WT cells, the cell suspension was adjusted to a cell density of $\sim 3x10^6$ cells/ml and 4ml was then placed on a series of 60mm plates with 1% agar. After a couple of minutes any excess liquid was drained and the cells were then left to starve for approximately 5 hours. Agar plates were left in the refrigerator if a longer development time – perhaps for testing subsequent conditions – was required. At the onset of streaming plates were harvested, the cells washed and resuspended with 2mM caffeine - to supress further cAMP secretion – at $\sim 6x10^5$ cells/ml. Cells were then left to settle on 22mm$^2$ slides, using 200μl suspension, for 20 minutes before being used in an Insall chamber assay.

For *aca*A$^-$ cells, the cell suspension was adjusted to a cell density of $\sim 1x10^7$ cells/ml and 10ml was then placed into a small flask. As these cells do not secrete cAMP they cannot develop via the usual method of starvation induced cAMP relays; instead they must instead be treated with external pulses of cAMP. The suspension was mixed on a rotating table for 1 hour, so the cells consume any residual bacteria and begin to starve, then treated with 300nM cAMP every 6 minutes for 4 hours, while still being mixed. Cells were then washed and resuspended – without caffeine – at $\sim 6x10^5$ cells/ml. Cells were then left to settle on slides as with WT above, before use in an Insall chamber.

### Chemotaxis chamber assays

Insall chambers & their use are described in Muinonen-Martin et al.[35] In all uses, buffer containing the chemical conditions required for the inner well was initially placed everywhere. The coverslip with cells adhered was then placed over the chamber, keeping the tips of the outer well free. The buffer in the outside well was replaced by new buffer containing the chemical conditions required for the outer well. If using WT cells the chemical condition containing buffers also included 2mM caffeine. The chamber was then left to equilibrate for around 15 minutes before filming the cells on the bridge of the chamber using a 10x objective in a Nikon Ti2 timelapse microscope with a Retiga R6 digital camera for around 20 minutes. This was sufficient time to obtain data on the directional bias at different point along the gradient at equilibrium.

A detailed protocol can be found in Muinonen-Martin et al.[44]

### Micropipette Assays

For this assay only WT cells were used; they were prepared as for chemotaxis chambers until the developing cells were at the onset of streaming, then harvested, washed and resuspended in 2ml of buffer. Enough suspension to give an appropriately low cell density was placed in a 35mm glass bottom dish containing no caffeine, caffeine or caffeine plus 2μM Sp-cAMPS. The micro-pipette (Eppendorf Nanotip Gold) was loaded with 10mM 8-CPT-cAMP, pressurized and lowered gently into the suspension. Images were recorded on an Olympus microscope at 10x magnification.

### Simulations

Simulations run are based on a Java code written by Tweedy et al.,[25] modified according to the needs of the project. Modifications include: inclusion of up to three competing chemicals of varying intrinsic efficacies, a rendering scheme illustrating the rate of change receptor activation with space and the possibility of accounting for chemical degradation in the wells due to cells located there. See also Methods S1.

### Wild-Type NC4 Bridge Chamber Assays

Cells were starved on agar for approximately 4 hours, examined, and harvested when centres of cell aggregation were visible across the plate, but before cells had started to stream. At this time the cells were harvested from a plate using 1ml KK2, washed into 1ml KK2MC, and diluted 15x into another 1ml KK2MC + 2mM caffeine. After mixing thoroughly once more, 200μl suspension was pipetted onto 22mm$^2$ cover slips and allowed to settle for at least 20 minutes before assembling the chamber. This was then left for about 10 minutes for the gradients to equilibrate before filming the 1mm bridge using a 10x objective in a Nikon Ti2 timelapse microscope with a Retiga R6 digital camera for around 20 minutes. This was sufficient time to obtain data on the directional bias at different point along the gradient at equilibrium.

## QUANTIFICATION AND STATISTICAL ANALYSIS

Data from live cell imaging was analysed using an ImageJ plugin,[25] giving positional data of cells at different time points. This data were converted into an X-direction velocity and average position for each tracked cell, such that an average velocity and error on the velocity could be found for each cell occupying a defined partition of the bridge.

Due to inter-experiment variability, local cell speeds or velocities were plotted as mean ±SE of cells at the indicated location in a single representative experiment; all experiments were repeated at least three times on different days, with consistent results. SE data are included in the figure legend where appropriate.